The local electronic structure of α -Li 3 N

T. T. Fister, G. T. Seidler, E. L. Shirley, F. D. Vila, J. J. Rehr, K. P. Nagle, J. C. Linehan, and J. O. Cross

Citation: The Journal of Chemical Physics **129**, 044702 (2008); doi: 10.1063/1.2949550
View online: http://dx.doi.org/10.1063/1.2949550
View Table of Contents: http://scitation.aip.org/content/aip/journal/jcp/129/4?ver=pdfcov
Published by the AIP Publishing

The local electronic structure of α-Li_3N

T. T. Fister,[1,2] G. T. Seidler,[1,a)] E. L. Shirley,[3] F. D. Vila,[1] J. J. Rehr,[1] K. P. Nagle,[1] J. C. Linehan,[4] and J. O. Cross[5]
[1]*Physics Department, University of Washington, Seattle, Washington 98195, USA*
[2]*Materials Science Division, Argonne National Laboratory, Argonne, Illinois 60439, USA*
[3]*National Institute of Standards and Technology, Gaithersburg, Maryland 20899-8441, USA*
[4]*Pacific Northwest National Laboratory, Richland, Washington 99352, USA*
[5]*Advanced Photon Source, Argonne National Laboratory, Argonne, Illinois 60439, USA*

(Received 11 January 2008; accepted 30 May 2008; published online 23 July 2008)

New theoretical and experimental investigations of the occupied and unoccupied local electronic densities of states (DOS) are reported for α-Li_3N. Band-structure and density-functional theory calculations confirm the absence of covalent bonding character. However, real-space full-multiple-scattering (RSFMS) calculations of the occupied local DOS find less extreme nominal valences than have previously been proposed. Nonresonant inelastic x-ray scattering, RSFMS calculations, and calculations based on the Bethe–Salpeter equation are used to characterize the unoccupied electronic final states local to both the Li and N sites. There is a good agreement between experiment and theory. Throughout the Li 1*s* near-edge region, both experiment and theory find strong similarities in the *s*-and *p*-type components of the unoccupied local final DOS projected onto an orbital angular momentum basis (*l*-DOS). An unexpected, significant correspondence exists between the near-edge spectra for the Li 1*s* and N 1*s* initial states. We argue that both spectra are sampling essentially the same final DOS due to the combination of long core-hole lifetimes, long photoelectron lifetimes, and the fact that orbital angular momentum is the same for all relevant initial states. Such considerations may be generally applicable for low atomic number compounds. © *2008 American Institute of Physics*. [DOI: 10.1063/1.2949550]

I. INTRODUCTION

Solid-state lithium nitrides and their immediate derivatives demonstrate a rich diversity[1] of bonding characteristics and crystal structures which has in turn led to both fundamental interest and a considerable range of potential applications. For example, α-Li_3N serves as the starting point for potential hydrogen storage methods due its high theoretical H_2 capacity[2] and also is a component in the synthesis of nanophase GaN.[3] In addition, its related transition-metal (M) substituted compounds,[4] $Li_{3-x}M_xN$, are excellent ionic conductors (as is α-Li_3N itself[1,5]) and have been proposed as constituents of improved electrodes in Li-based batteries.[6]

After significant investigation and dispute, the chemical bonding of α-Li_3N is now understood to be near the extreme ionic end point of the continuum from covalent to ionic behavior.[1] It is the only alkali-nitride phase which is stable at ambient conditions,[7,8] and it is interesting that several estimates of the nominal classical valences of the constituents are close to Li^+ and N^{3-}.[1] Consequently, α-Li_3N, and possibly its high-pressure phases,[8–10] are believed to provide the only known examples of the N^{3-} ion. N^{3-} is not stable as a free ion, and the mechanism by which the hexagonal bipyramid of neighboring Li^+ may stabilize N^{3-} in α-Li_3N has been a matter of some interest.[1,9,11–13] For means of context, we show the crystal structure[14] of α-Li_3N in the top panel of Fig. 1. Note the layered structure and the presence of two crystallographically distinct Li sites.

Here, we revisit the local electronic structure in α-Li_3N. First, using band-structure, density-functional theory (DFT), and real-space full-multiple-scattering (RSFMS) methods, we consider the occupied electronic states. The former two calculations find strong support for extremely ionic bonding character in α-Li_3N. The weak deviations from sphericity in the calculated valence charge distribution around N show no sign of covalent character with the Li nearest neighbors. By common measures, such as integration of valence charge density within nominal ionic radii, the charge transfer from Li to N is at least nearly complete. However, calculation of charge transfer based on RSFMS calculation of the occupied local density of states (DOS) disagrees with the above, finding clear evidence for occupied states just below the Fermi energy at all crystallographic sites. We compare and contrast these results, emphasizing the difficulty in uniquely defining species valence and suggesting the need for experimental measurement of the occupied local DOS, such as by resonant x-ray photoemission spectroscopy.

Second, we report combined experimental and theoretical investigations of the unoccupied electronic states. Excited-state electronic spectroscopies such as x-ray absorption spectroscopy (XAS) and electron energy-loss spectroscopy (EELS) offer a local probe of the unoccupied electronic states and have been widely used to study the chemical bonding of low atomic number materials.[15] However, there has been little XAS or EELS work on α-Li_3N, with the few existing studies concentrating on the very near-edge region within less than 10 eV of the Li and N *K*-shell binding

a)Electronic mail: seidler@phys.washington.edu.

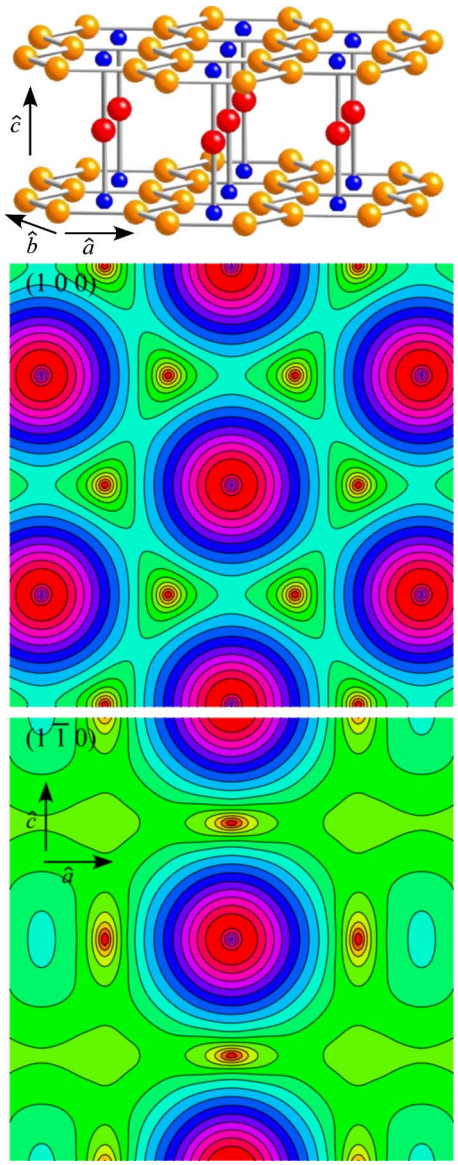

FIG. 1. (Color online) Top panel: A ball-and-stick schematic of the crystal structure of α-Li_3N. The small blue spheres represent N atoms in the Li_2N basal planes, while the larger orange and red spheres represent the in-plane (Li(1)) and out-of-plane (Li(2)) Li sites, respectively. Middle panel: The valence electron charge density for α-Li_3N in the (001) plane from band-structure calculations. Bottom panel: The valence electron charge density in the $(1\bar{1}0)$ plane from band structure calculations. The contours in these two panels are logarithmically spaced, and the central atom for both panels is N. In the middle panel, the outermost triangular contour around Li sites has $\rho_{\text{valence}}=10^{-2}$ electrons/Å^3 and the contours are spaced by $\Delta \log_{10} \rho_{\text{valence}}=0.2$ with ρ_{valence} again in units of electrons/Å^3. In the bottom panel, the outermost roughly square contour around the N site has $\log_{10} \rho_{\text{valence}}=-2.2$ and the contour spacing is $\Delta \log_{10} \rho_{\text{valence}}=0.2$ with ρ_{valence} in units of electrons/Å^3.

energies.[16,17] Nonresonant inelastic x-ray scattering (NRIXS) using hard x-rays provides an alternative which allows investigation of both dipole-allowed and dipole-forbidden final states while also avoiding the problematic surface sensitivity of soft x-ray XAS and the possibility of beam damage in EELS. The core shell contribution to NRIXS is generally called nonresonant x-ray Raman scattering (XRS). The first XRS study of the N *K*-edge in several phases of Li_3N has recently[9,18] been reported.

Here, we present the first measurements of the momentum transfer-(q-) dependence of the XRS from the Li 1*s* initial state and also present new measurements over a wider energy range of the effectively dipole-limit XRS from N 1*s* initial states. Our measurements of the Li 1*s* XRS allow experimental determination of the local final DOS projected onto an orbital angular momentum basis (i.e., the *l*-DOS) at the Li sites. All measurements show good agreement with new *ab initio* calculations. We find a strong similarity of the near-edge structure for the Li and N 1*s* XRS. Such behavior in XAS studies is often taken as a signature of covalent bonding. However, here we find that it is a generic consequence of the strong multiple-scattering limit for low-energy photoelectrons in cases when all core-hole lifetimes are much longer than the photoelectron lifetime and when all initial states have the same orbital angular momentum. Such conditions will, in general, hold for compounds of low atomic number elements.

II. THEORY

A. NRIXS

The double differential cross section for NRIXS is proportional to the dynamic structure factor

$$S(\vec{q},\omega)=\sum_f |\langle f|\exp(i\vec{q}\cdot\vec{r})|0\rangle|^2 \delta(\hbar\omega - E_f + E_0), \quad (1)$$

where $\vec{q}$ is the momentum transfer, $\hbar\omega$ is the energy transfer, and $E_0(E_f)$ is the energy of the initial (final) state. The contribution to $S(\vec{q},\omega)$ due to excitations from core levels is commonly called nonresonant XRS. Beyond the plasmon frequency and when in the dipole-scattering (i.e., low-q) limit, the XRS contribution to $S(\vec{q},\omega)$ becomes proportional to the absorption coefficient measured in XAS, albeit with bulklike sensitivity even for low-energy edges due to the large incident and scattering photon energies.[19,20]

Nondipole selection rules apply for $S(\vec{q},\omega)$ at higher q,[21,22] allowing investigation of the complete range of symmetries of final states at the probe atom.[20,22–27] For powder samples, the XRS contribution to $S(q,\omega)$ may be recast[22] as

$$S_{\text{core}}(q,\omega)=\sum_l (2l+1)|M_l(q,\omega)|^2 \rho_l(\omega). \quad (2)$$

In Eq. (2), the projection of the local final DOS onto an orbital angular momentum basis (i.e., the *l*-DOS) is represented by ρ_l. The atomic-like M_l coefficients may be readily calculated.[22] At each energy, Eq. (2) should therefore be viewed as a set of linear equations (one for each experimental q) involving experimental measurements of $S(q,\omega)$, the known M_l coefficients, and the unknown $\rho_l(\omega)$. As such, it gives a route for experimental determination of $\rho_l(\omega)$ from XRS measurements.[24,25,27,28] Here, we use this formalism to determine both the *s*-type (ρ_0) and *p*-type (ρ_l) *l*-DOS for Li in α-Li_3N. By comparison, XAS or low-q EELS measurements for the Li 1*s* initial state will be sensitive only to ρ_1 due to the dipole selection rule. The range of potential applications of this new *l*-DOS spectroscopy has recently been discussed in detail.[24]

B. Calculations of *l*-DOS and $S(q,\omega)$

Our experimental measurements of the excited electronic states are complemented by two independent *ab initio* theoretical treatments. In both cases, the potentials used in the calculations are determined self-consistently *without* any assumption about the valence of the constituent atoms. This is contrary to the some prior band-structure calculations[11] for α-Li_3N, where a N^{3-} ion was stabilized by use of an artificial potential prior to enforcing self-consistency.

First, a RSFMS approach using the FEFF code[29] was used to calculate the *l*-DOS and XRS spectra[22] [i.e., $S_{\mathrm{core}}(q,\omega)$]. The full-multiple-scattering matrix includes atoms up to 8 Å from the central scatterer using self-consistent muffin-tin potentials. For both parts of the calculation, the spectra are converged with respect to the number of atoms and the number of angular momentum states, which was limited to $l=2$. The default statically screened core-hole was used in the calculations. Finally, we include the effects of the core-hole lifetime and the photoelectron's self-energy in the final spectra. Note that independent calculations for the planar and out-of-plane Li atoms are required for comparison with the orientationally averaged data.

Second, XRS spectra were calculated using the Bethe–Salpeter equation (BSE), which is the equation of motion for an interacting electron-hole pair produced by core-electron excitation. We use the method described by Soininen *et al.*,[30] but with certain modifications. First, a model self-energy is used to simulate electron lifetime broadening of spectral features.[31] The screening effects on the electron-core hole interaction and the transition matrix elements are evaluated using methods that have been described in detail elsewhere.[32] Multiplet effects (related here only to spin degrees of freedom) are also included.[33] The bands are calculated using pseudopotential plane-wave methods using optimal basis functions.[34] Specifically, we use norm-conserving pseudopotentials of the Hamann–Schlüter–Chiang type[35] with Vanderbilt-type cutoff functions[36] and separable projectors.[37] Other details of the calculation method follow prior work.[30] All results are well converged with respect to Brillouin-zone sampling, with enough unoccupied bands included to calculate screening effects and spectra within and beyond the displayed region. Because of the threefold symmetry with respect to the *z*-axis, angular averaging over the direction of $\vec{q}$ was achieved using a momentum along the Cartesian (1,1,1) direction. The final theoretical results are convolved with experimental broadening (1.3 eV full width at half maximum).

C. Calculations of electron density and occupied electronic states

The spatial distribution of valence electron density has been calculated in two independent ways. First, it is determined from superposition of the density associated with the bands calculated as a preliminary step in the BSE approach described above. Second, we have performed DFT calculations on the experimentally determined structure of α-Li_3N using ultrasoft pseudopotentials and a plane-wave basis set. These calculations were carried out with the Vienna *ab initio* simulation package[38] (VASP) using the Perdew–Burke–Ernzerhof functional[39] and an energy cutoff of 350 eV. The Bader decomposition[40] of the electron density uses the algorithm introduced by Henkelman *et al.*[41]

The occupied local DOS on each crystallographic site was calculated with the same RSFMS approach as presented in Sec. II B, except that no core hole was included in the calculations. The valence electron density and unoccupied local DOS calculations provide complementary benefits and perspectives as regards the question of charge transfer, as we discuss below.

III. EXPERIMENTAL

All NRIXS measurements were performed with the lower energy resolution inelastic x-ray (LERIX) scattering spectrometer at the PNC/XOR 20-ID beamline of the Advanced Photon Source.[42] Spectral normalization, subtraction of the valence Compton background, and other data processing issues follow methods reported elsewhere.[23,43] The energy resolution was 1.3 eV. A dense 5 mm-thick pellet of commercially prepared α-Li_3N powder (99% purity) was measured in a transmission geometry. Note that the 5 mm thickness is chosen to match the penetration length of α-Li_3N at 10 keV. With such a large penetration length, our measurements are inherently bulklike with no sensitivity to surface contamination. While commercial Li_3N typically contains a small fraction of metastable β-Li_3N impurity, the bulk sensitivity of XRS ensures that the measured signal is dominated by the desired α-Li_3N phase.

The incident flux of photons was about 5×10^{12} s^{-1}. The count rates at the edges and in the underlying valence Compton background are strong functions of q. At $q=2.4$ $Å^{-1}$ we find 6100 and 230 counts/s at the Li- and N *K*-edge steps on valence Compton scattering backgrounds of 17 000 and 220 counts/s, respectively. Increasing q to 9.8 $Å^{-1}$ resulted in 2100 and 1300 counts/s at the Li- and N *K*-edge steps on valence Compton scattering backgrounds of 1100 and 31000 counts/s, respectively. Following these measurements we found a significant air leak into the He flight path (outside the sample space) of the instrument. This resulted in a decrease in all count rates by a factor of about 3.5 compared to present LERIX performance, but otherwise has no consequences for the results presented here. The sample was enclosed in a flowing He environment during measurements. The XRS spectra show no evidence of evolution with measuring time, minimizing concerns about beam damage.

IV. RESULTS AND DISCUSSION

A. Occupied electronic states

The highly ionic nature of α-Li_3N plays an important role in the interpretation of NRIXS results (below). As there has been significant progress in computational methods in the several years since the spatial distribution of electron density was last directly investigated for this system,[11–13] it is worthwhile to revisit this issue. In the middle and bottom panels of Fig. 1, we show the calculated valence electron density in the Li_2N basal plane (001) and the normal plane

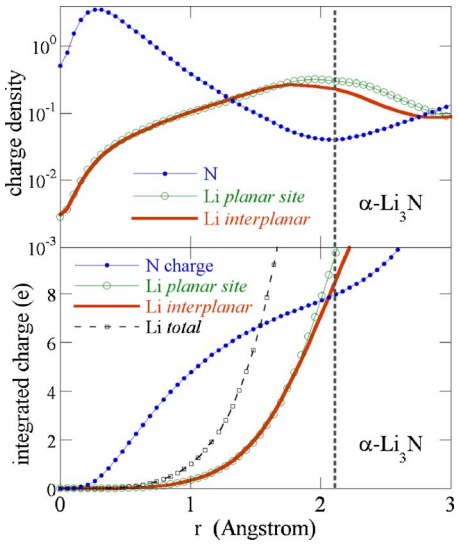

FIG. 2. (Color online) (Top) The directional average of the calculated valence charge density around each crystallographic site in α-Li_3N, based on the band-structure calculation. The units for the plot are electrons/Å^3. (Bottom) The integrated charge as a function of radial distance around each atomic site. The vertical dashed line indicates the nearest-neighbor Li–N distance in the Li_2N basal plane.

$(1\bar{1}0)$ based on the new band-structure calculations. The contours are on a logarithmic scale, as explained in the caption. The valence charge density is nearly spherical around the N sites. Note that the first deviations from sphericity show a weak excess of charge density in the N–N nearest-neighbor direction, not the N–Li direction, so that even at low valence charge densities there is no signature of covalent character. The valence charge density is essentially zero at the Li nuclei and decreases monotonically and nearly exponentially after a local maximum near the N nuclei.

This can be seen more clearly in the top panel of Fig. 2 which shows the directionally averaged valence charge density as a function of distance from the three crystallographic sites. The vertical dashed line in the figure is at the Li–N nearest-neighbor distance in the Li_2N sheets. The bottom panel of the figure shows the integrated valence charge as a function of distance from the three crystallographic sites, together with the total Li-site charge. These results strongly support a very ionic picture for the chemical bonding in α-Li_3N and are very similar to prior band-structure based results.[11,13]

This conclusion is further supported by the calculations of the α-Li_3N valence electron density calculated with the DFT/VASP approach. The electron density around the N atoms is very close to spherically symmetric, even in regions close to the Li atoms. Small deviations are visible on the basal plane and have the same characteristics as seen in the band-structure calculations. When the electron density distribution is analyzed using the "atoms in molecules" scheme of Bader,[40] we find that the dividing surfaces are pushed into the Li atom positions, resulting in a highly ionic distribution.

However, it is important to remember that the valence charge of a particular species in a solid is not itself well defined. Any correct approach to the question of charge transfer must explicitly address a quantum mechanical (i.e., experimental) observable, and the final estimate of charge transfer may indeed depend on the choice of observable. In Fig. 3, we present RSFMS calculations of the occupied local DOS for cells surrounding each of the three crystallographic sites. The key feature of these results is not just the presence of large N $2p$ DOS just below E_F but also the presence of significant DOS at similar energies for both Li sites. The occupied charge counts are quite different from what was qualitatively inferred from our density-functional calculations (both those carried out to compute the band structure for purposes of the Bethe–Salpeter calculations or those done using VASP) or from prior band-structure calculations[11–13] because they refer to the contributions of the global DOS projected onto the given cells. The RSFMS calculations provide nominal valences of $N^{-0.9}$ and $Li^{+0.3}$, with slightly higher ionization of the out-of-plane Li site and slightly lower ionization at the in-plane Li site.

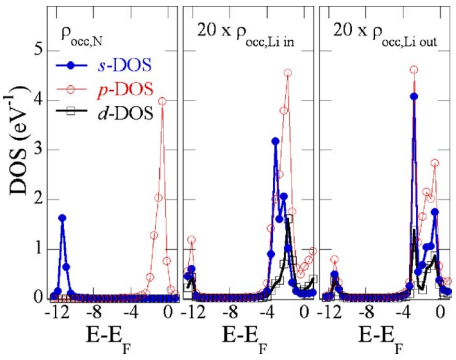

FIG. 3. (Color online) RSFMS calculations of the occupied l-DOS for N (left), the in-plane Li site (center), and the out-of-plane Li site (right).

This significantly lower estimate of charge transfer may help resolve a dilemma which has been noted in comparing the electronic structures of α-, β-, and γ-Li_3N.[9] In the study of Lazicki *et al.*,[9] it was proposed that high-pressure γ-Li_3N must be significantly more ionic than α- or β-Li_3N due to a large increase in the band gap. However, this is difficult to rationalize if α-Li_3N already has complete ionization of all species in addition to the absence of covalent bonding character. In future work, it would be interesting to consider how strongly the nominal valence of the various species depends on the definition of the local DOS. For example, it would clearly be valuable to have direct experimental measurement of the element-specific occupied DOS, such as by resonant x-ray photoemission spectroscopy.[44]

B. Excited electronic states

With the above reinforcement that chemical bonding in α-Li_3N does indeed have very little covalent character, we proceed to present and discuss the new experimental results. In the top of Fig. 4, we show Li $1s$ XRS spectra for q=0.8, 2.4, 3.9, 5.3, 6.6, 7.7, 8.6, 9.3, 9.8, and 10.1 Å^{-1}. Counts are integrated for 9 s at each point. The corresponding BSE calculations are shown in the lower panel. To aid comparison, the energy-loss spectra have been normalized by their integrated intensity over the first 30 eV and are vertically displaced between successive q. Several features in the near-edge spectrum are labeled (a–f in Fig. 4) to highlight the

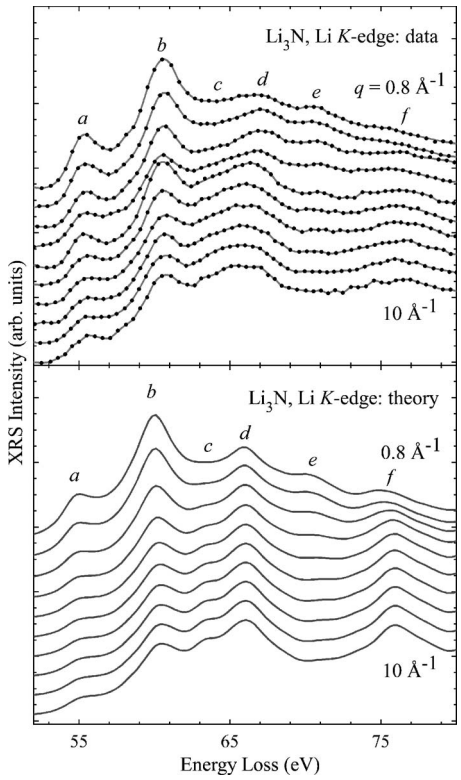

FIG. 4. The Li 1*s* contribution to $S(q,\omega)$ for α-Li_3N. Top panel: Experimental results stacked by q and normalized to aid comparison. Statistical errors are comparable to the size of the dots used in the figure. Bottom panel: Analogous BSE results with additional broadening from the experimental resolution and the self-energy of the photoelectron. The first six notable features are labeled $a-f$ to highlight the agreement between experiment and theory.

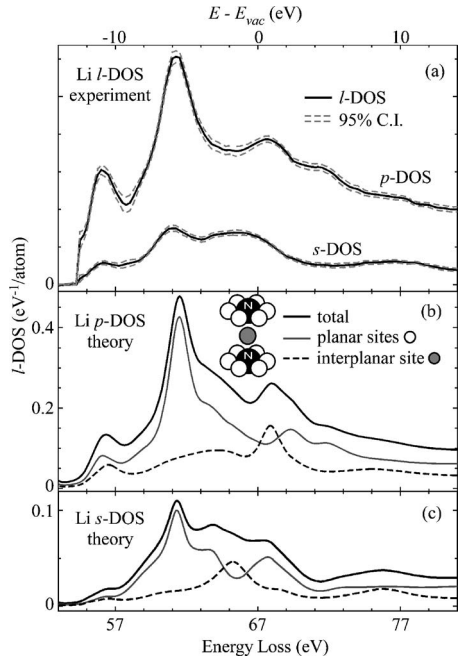

FIG. 5. (a) The experimental Li *s*- and *p*-DOS ($l=0$ and 1, respectively) given by inverting the results shown in Fig. 4. Shown by gray dashed lines, the 95% confidence interval is given by the quality of the least-squares fit to Eq. (2) at each energy point; (b) the total theoretical *p*-DOS is given by the dark curve, while the contributions from the planar and interplanar sites are given by the gray and dashed curves, respectively; (c) the analogous figure for the theoretical *s*-DOS.

agreement between theory and experiment. Note that each of these features exhibit modest q dependence, with *a*, *b*, and *e* decreasing in relative amplitude with q, while *c*, *d*, and *f* either increase or only appear at higher momentum transfers. Each feature corresponds to a peak in the unoccupied final DOS local to each Li atom, albeit with each possessing differing local symmetry. Such q dependence in localized features can be interpreted as changes in the relative weighting of the different l-DOS components.[22,24] We note that the XRS spectrum for the lowest measured q disagrees significantly with recent XAS results.[16] The bulk sensitivity of XRS, the good agreement between theory and experiment, and the preferential surface sensitivity of XAS with soft x-rays give us confidence in the present results.

On calculating $M_l(q,\omega)$ for the Li 1*s* initial state,[22,43] we find that only the *s*-and *p*-DOS ($l=0$ and 1, respectively) significantly contribute to $S(q,\omega)$. After normalizing the data shown in Fig. 4 to absolute units, we extract ρ_0 and ρ_1 at each energy point in the near-edge regime using a least-squares fit to the model given by the first two terms in Eq. (2).[24,43] The M_l coefficients were found to be nearly identical for the two crystallographically independent Li sites; hence, only the stoichiometrically averaged l-DOS from both sites can be obtained by inverting the experimental results via Eq. (2). These results are shown in Fig. 5(a). The RSFMS calculations for the *p*-DOS and *s*-DOS are shown in Figs. 5(b) and 5(c), respectively. The agreement between the experimental and calculated l-DOS is relatively good, with discrepancies mainly in the relative amplitude of features. Such disagreements are to be expected in the present RSFMS approach due to the details of the treatment of the electron-core hole interaction and perhaps especially due to our decision to not force the effective radius of the N to grow and of the Li to shrink, e.g., as is needed to artificially force agreement with the expectation of a large nominal N ionic radius, such as is seen in Figs. 1 and 2. Future RSFMS work based on a full-potential calculation should remedy this deficiency.

Some aspects of the experimental and theoretical l-DOS deserve special attention. Except for an overall scale factor, the experimentally determined *s*- and *p*-DOS are quite similar for the first 15 eV. The theoretical l-DOS calculations show similar agreement, but clarify that this phenomenon occurs independently for each of the two Li sites. Commonality of isolated features in the l-DOS can be taken as a significant fingerprint for covalency, such as from a shared DOS from a hybridized antibonding molecular orbital.[24,25] However, it is important to recall that localization of the occupied states near the Fermi energy does not as a rule constrain the spatial extent and overlap of the unoccupied states near the Fermi energy. The general agreement in structures of the *s*-and *p*-DOS is a direct signature of significant overlap and hybridization of the low-energy unoccupied final states, without any specific conclusions to be drawn about the degree of localization (i.e., nominal ionicity versus covalency) of the occupied states. Given the threefold and sixfold rotational symmetries about the respective Li sites, a significant degree of *s*-*p* hybridization of low-lying unoccupied states is not surprising. The consistency between the l-DOS

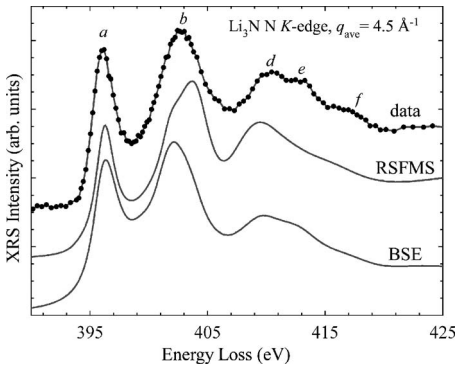

FIG. 6. The N 1*s* contribution to $S(q,\omega)$ for α-Li_3N. Top curve: Experimental results averaged between $q=2.4$ and 5.3 Å^{-1}. Standard uncertainties are comparable to the size of the dots used in the figure. Bottom curves: Theoretical results from RSFMS and BSE calculations.

calculations for the occupied states (Fig. 3) and the present results on the unoccupied states is still worth noting: it is difficult to imagine a scenario where hybridization of occupied states would not be similarly accompanied by hybridization of unoccupied states.

We show experimental and theoretical results for the N 1*s* XRS in Fig. 6. Counts are integrated for 5 s at each incident photon energy, and each point represents the weighted average of energy-loss spectra collected at $q=2.4$, 3.9, and 5.3 Å^{-1}. The q range for LERIX is insufficient for *l*-DOS determination at the N sites, and the results are dominated by transitions to *p*-type final states (i.e., dipole-limited transitions); this is due to the smaller size of the N 1*s* initial state as compared to the Li 1*s* initial state. Note that the very near-edge spectrum is in fair agreement with prior XRS measurement[9,18] having poorer counting statistics but is in disagreement with prior EELS measurement,[17] which we attribute to likely electron beam damage. The agreement with the RSFMS and BSE calculations (solid lines in Fig. 6) is quite good, as is the agreement with the recent calculations of Lazicki *et al.*, using related methods.[18]

In Table I we show a comparison of the peak positions for the Li and N 1*s* XRS spectra, i.e., from Figs. 4 and 6. The agreement in the energy spacing between the first and second features is quite good, and the simple fact of a significant feature at the edge and only one other broad feature in the first 10 eV should not be overlooked. Continuing to higher energies, the absence of peak (*c*) in the N XRS spectrum is expected in this picture: that peak is due to *s*-type final states which are inaccessible at the N *K*-edge for our available q range when using ~10 keV incident photons. The modest energy shifts of peaks (*d*) and (*e*) may be due to differences in the self-energy effects for the two different species.

TABLE I. A comparison of the energies and energy spacings for the principal features observed in the Li and N 1*s* XRS spectra for α-Li_3N, as per Figs. 4 and 6. Feature *c* occurs only in the Li XRS spectra as a consequence of nondipole selection rules at high momentum transfer.

	Li 1*s*		N 1*s*	
Feature	E (eV)	$E-E_a$ (eV)	E (eV)	$E-E_a$ (eV)
a	55.3	0	396.0	0
b	60.6	5.3	402.6	6.6
c	63.3	8.0	…	…
d	67.1	11.8	410.4	14.4
e	70.7	15.4	413.3	17.3
f	76.5	21.2	417.0	21.0

The peak matching of the Li and N 1*s* near-edge spectra indicates that they result from different sampling of a shared, underlying DOS. This is most often seen in XAS spectra for systems with strong covalent bonding, where strong, localized, multiple-scattering resonances (i.e., antibonding orbitals) necessarily span neighboring crystallographic sites and result in peak matching in the near-edge spectra. However, we propose that this behavior is independent of the details of chemical bonding, subject only to the condition that the core-hole and photoelectron lifetimes are large.

Most generally, in the limit of long lifetimes the x-ray absorption coefficient $\mu_j(E)$ at a crystallographic site j is

$$\mu_j(E) = \sum_k \langle j|d|k,\bar{j}\rangle \delta(E-E_k)\langle k,\bar{j}|d|j\rangle, \tag{3}$$

where k is the photoelectron momentum, d is the dipole transition operator, $|k,\bar{j}\rangle$ is the photoelectron wave function for momentum k including final state effects from the core hole at site j, and $|j\rangle$ denotes the initial state, localized orbital at site j. Core-hole effects are relatively small in the limit of long lifetimes because the photoelectron wave function will be spatially extended. Hence, in this limit,

$$\mu_j(E) \approx \sum_k |\langle k|d|j\rangle|^2 \delta(E-E_k). \tag{4}$$

As $|f_j\rangle \equiv d|j\rangle$ is simply the dipole-allowed final states accessible from $|j\rangle$,

$$\mu_j(E) \approx \sum_k |\langle k|f_j\rangle|^2 \delta(E-E_k) = \langle f_j|\rho^{\text{global}}(E)|f_j\rangle, \tag{5}$$

where $\rho^{\text{global}}(E)$ is the (global) DOS for the system. For 1*s* initial states, such as here, the same orbital angular momentum-projected component of $\rho^{\text{global}}(E)$ will be important for all sites, i.e., the *p*-type component $\rho_1^{\text{global}}(E)$. The near-edge spectra are therefore expected to be similar, with differences in the relative amplitude of near-edge features due to the fine spatial details of the expectation integrand in Eq. (5). As an extreme case, for example, note that geometric arrangements (such as three-atom collineations[45]) which strongly favor particular high-order multiple-scattering paths will lead to differences in $\mu_j(E)$ between sites involved in such paths and those independent of such paths. Modest differences in the relative locations of peaks may be caused by the site- and final-state-specific nature of the interaction between the core-hole and photoelectron.

Independent of the nature of their chemical bonding, compounds of low Z elements will necessarily have long core-hole lifetimes for the 1*s* initial state, and the above argument should be relevant in the near-edge region when the photoelectron lifetime is also relatively large. As photoelectron energy increases this mechanism is cut off by the increase in extrinsic losses and consequent decrease in photoelectron lifetime,[46] so that $|k,\bar{j}\rangle$ and the fine structure then become sensitive to the source site. We therefore anticipate

that significant commonality in the XAS, EELS, or dipole-limit XRS near-edge structure at different crystallographic sites may be routinely observed in low Z systems when the selected initial states at all sites have the same orbital angular momentum. When outside of the dipole limit, the different admixtures of final state symmetries present in the XRS spectra may result in unique spectral features, such as is the case for feature (c) in the Li XRS of the present study.

V. CONCLUSIONS

In conclusion, we report measurement and *ab initio* calculation of the local electronic structure of α-Li_3N. First, band-structure and DFT calculations reinforce that chemical bonding in α-Li_3N has little covalent character. Interestingly, RSFMS calculations of nominal valences based on a quantum mechanical observable, the local final density of occupied states, find relatively modest charge transfers resulting in $N^{-0.9}$ and $Li^{+0.3}$ ions. This is contrary to more empirical measures of nominal valence, such as from integrating the calculated valence charge density in a selected ionic radius. Second, we find good agreement between theory and both the excited state spectra from the Li- and N K-edges and also the resulting experimentally-determined l-DOS. We find a strong correspondence between the Li s- and p-DOS in both experiment and calculations, which is a direct indicator of strong hybridization of low-lying unoccupied states. Third, we observe that the N and Li 1s near-edge structures are very similar, indicating that they are sampling a common underlying DOS. We propose a new explanation for such behavior which is based on the long core-hole lifetime for low atomic number systems and the extreme multiple-scattering limit for low-energy photoelectrons. This mechanism should be active in many other materials, independent of whether their chemical bonding is ionic or covalent.

ACKNOWLEDGMENTS

This research was supported by the U.S. Department of Energy, Basic Energy Science, Office of Science, Contract Nos. DE-FGE03-97ER45628 and W-31-109-ENG-38, Office of Naval Research Grant No. N00014-05-1-0843, and the Summer Research Institute program at the Pacific Northwest National Laboratory. The operation of Sector 20 PNC-CAT/XOR is supported by the U.S. Department of Energy, Basic Energy Science, Office of Science, Contract No. DE-FG03-97ER45629, the University of Washington, and grants from the Natural Sciences and Engineering Research Council of Canada. Use of the Advanced Photon Source was supported by the U.S. Department of Energy, Basic Energy Sciences, Office of Science, under Contract No. DE-AC02-06CH11357. We thank Ed Stern, Warren Pickett, Micah Prange, Joshua Kas, and J. Aleksi Soininen for helpful discussions.

[1] D. H. Gregory, Coord. Chem. Rev. **215**, 301 (2001).
[2] Y. H. Hu and E. Ruckenstein, J. Phys. Chem. A **107**, 9737 (2003); Y. H. Hu and E. Ruckenstein, Ind. Eng. Chem. Res. **42**, 5135 (2003); Y. H. Hu, N. Y. Yu, and E. Ruckenstein, *ibid.* **43**, 4174 (2004); Y. H. Hu, N. Y. Yu, and E. Ruckenstein, *ibid.* **44**, 4304 (2005); H. M. Jin, J. Z. Luo, and P. Wu, Appl. Phys. Lett. **90**, 084101 (2007); H. W. Langmi and G. S. McGrady, Coord. Chem. Rev. **251**, 925 (2007); K. Miwa, N. Ohba, S. Towata, Y. Nakamori, and S. Orimo, Phys. Rev. B **71**, 195109 (2005); Y. Nakamori and S. Orimo, Mater. Sci. Eng., B **108**, 48 (2004); S. I. Orimo, Y. Nakamori, J. R. Eliseo, A. Zuttel, and C. M. Jensen, Chem. Rev. (Washington, D.C.) **107**, 4111 (2007); Y. Song and Z. X. Guo, Phys. Rev. B **74**, 195120 (2006).
[3] Y. Xie, Y. T. Qian, W. Z. Wang, S. Y. Zhang, and Y. H. Zhang, Science **272**, 1926 (1996).
[4] Z. Stoeva, R. I. Smith, and D. H. Gregory, Chem. Mater. **18**, 313 (2006); A. G. Gordon, D. H. Gregory, A. J. Blake, D. P. Weston, and M. O. Jones, Int. J. Inorg. Mater. **3**, 973 (2001); A. G. Gordon, R. I. Smith, C. Wilson, Z. Stoeva, and D. H. Gregory, Chem. Commun. (Cambridge) **24**, 2812 (2004); D. H. Gregory, P. M. O'Meara, A. G. Gordon, J. P. Hodges, S. Short, and J. D. Jorgensen, Chem. Mater. **14**, 2063 (2002); P. Novak and F. R. Wagner, Phys. Rev. B **66**, 184434 (2002).
[5] E. Bechtoldschweickert, M. Mali, J. Roos, and D. Brinkmann, Phys. Rev. B **30**, 2891 (1984); S. Ihara and K. Suzuki, Phys. Lett. A **110**, 265 (1985); M. L. Wolf and C. R. A. Catlow, J. Phys. C **17**, 6635 (1984); J. Sarnthein, K. Schwarz, and P. E. Blochl, Phys. Rev. B **53**, 9084 (1996); M. L. Wolf, J. Phys. C **17**, L285 (1984); A. Rabenau, Solid State Ionics **6**, 277 (1982).
[6] D. Aurbach, E. Zinigrad, H. Teller, Y. Cohen, G. Salitra, H. Yamin, P. Dan, and E. Elster, J. Electrochem. Soc. **149**, A1267 (2002); Z. W. Fu, Y. Wang, X. L. Yue, S. L. Zhao, and Q. Z. Qin, J. Phys. Chem. B **108**, 2236 (2004); Y. Liu, K. Horikawa, M. Fujiyosi, N. Imanishi, A. Hirano, and Y. Takeda, J. Electrochem. Soc. **151**, A1450 (2004); Y. Liu, K. Horikawa, M. Fujiyosi, N. Imanishi, A. Hirano, and Y. Takeda, Electrochim. Acta **49**, 3487 (2004); Y. Liu, T. Matsumura, N. ImanishI, T. Ichikawa, A. Hirano, and Y. Takeda, Electrochem. Commun. **6**, 632 (2004); Y. Liu, Y. Takeda, T. Matsumura, J. Yang, N. Imanishi, A. Hirano, and O. Yamamoto, J. Electrochem. Soc. **153**, A437 (2006); H. Sun, X. M. He, J. J. Li, J. G. Ren, C. Y. Jiang, and C. R. Wan, Solid State Ionics **177**, 1331 (2006); L. Wang, X. M. He, W. H. Pu, C. Y. Jiang, and C. R. Wan, Progress in Chemistry **18**, 641 (2006).
[7] D. Fischer, Z. Cancarevic, J. C. Schon, and M. Jansen, Z. Anorg. Allg. Chem. **630**, 156 (2004); J. C. Schon, M. A. C. Wevers, and M. Jansen, Solid State Sci. **2**, 449 (2000); G. V. Vajenine, Inorg. Chem. **46**, 5146 (2007).
[8] J. C. Schon, M. A. C. Wevers, and M. Jansen, J. Mater. Chem. **11**, 69 (2001).
[9] A. Lazicki, B. Maddox, W. J. Evans, C. S. Yoo, A. K. McMahan, W. E. Pickett, R. T. Scalettar, M. Y. Hu, and P. Chow, Phys. Rev. Lett. **95**, 165503 (2005).
[10] H. J. Beister, S. Haag, R. Kniep, K. Strossner, and K. Syassen, Angew. Chem., Int. Ed. Engl. **27**, 1101 (1988); A. C. Ho, M. K. Granger, A. L. Ruoff, P. E. Van Camp, and V. E. Van Doren, Phys. Rev. B **59**, 6083 (1999).
[11] P. Blaha, J. Refinger, and K. Schwarz, Z. Naturforsch. B **57**, 273 (1984); P. Blaha, K. Schwarz, and P. Herzig, Phys. Rev. Lett. **54**, 1192 (1985).
[12] R. Dovesi, C. Pisani, F. Ricca, C. Roetti, and V. R. Saunders, Phys. Rev. B **30**, 972 (1984).
[13] G. Kerker, Phys. Rev. B **23**, 6312 (1981).
[14] A. Rabenau and H. Schulz, J. Less-Common Met. **50**, 155 (1976).
[15] J. Stohr, *NEXAFS Spectroscopy* (Springer, Berlin, 1992).
[16] A. Braun, H. X. Wang, J. Shim, S. S. Lee, and E. J. Cairns, J. Power Sources **170**, 173 (2007).
[17] S. Suzuki, T. Shodai, and J. Yamaki, J. Phys. Chem. Solids **59**, 331 (1998).
[18] A. Lazicki, C. S. Yoo, W. J. Evans, M. Y. Hu, P. Chow, and W. E. Pickett, "Pressure-induced loss of electronic interlayer state and metallization in ionic solid ," Phys. Rev. B (submitted).
[19] M. Balasubramanian, C. S. Johnson, J. O. Cross, G. T. Seidler, T. T. Fister, E. A. Stern, C. Hamner, and S. O. Mariager, Appl. Phys. Lett. **91**, 031904 (2007); U. Bergmann, A. DiCicco, P. Wernet, E. Principi, P. Glatzel, and A. Nilsson, J. Chem. Phys. **127**, 174504 (2007); U. Bergmann, P. Glatzel, and S. P. Cramer, Microchem. J. **71**, 221 (2002); M. Krisch and F. Sette, Surf. Rev. Lett. **9**, 969 (2002); S. K. Lee, P. J. Eng, H. K. Mao, Y. Meng, M. Newville, M. Y. Hu, and J. F. Shu, Nat. Mater. **4**, 851 (2005); W. L. Mao, H. K. Mao, P. J. Eng, T. P. Trainor, M. Newville, C. C. Kao, D. L. Heinz, J. F. Shu, Y. Meng, and R. J. Hemley, Science **302**, 425 (2003); W. Schulke, K. J. Gabriel, A. Berthold, and H. Schulteschrepping, Solid State Commun. **79**, 657 (1991); H. Sternemann, C. Sternemann, J. S. Tse, S. Desgreniers, Y. Q. Cai, G. Vanko, N. Hiraoka, A. Schacht, J. A. Soininen, and M. Tolan, Phys. Rev. B **75**,

245107 (2007); K. Tohji and Y. Udagawa, *ibid.* **36**, 9410 (1987); K. Tohji and Y. Udagawa, *ibid.* **39**, 7590 (1989); N. Watanabe, H. Hayashi, Y. Udagawa, K. Takeshita, and H. Kawata, Appl. Phys. Lett. **69**, 1370 (1996); Ph. Wernet, D. Nordlund, U. Bergmann, M. Cavalleri, M. Odelius, H. Ogasawara, L. A. Naslund, T. K. Hirsch, L. Ojamae, P. Glatzel, L. G. M. Pettersson, and A. Nilsson, Science **304**, 995 (2004).
[20] H. Sternemann, J. A. Soininen, C. Sternemann, K. Hamalainen, and M. Tolan, Phys. Rev. B **75**, 075118 (2007).
[21] Y. J. Feng, G. T. Seidler, J. O. Cross, A. T. Macrander, and J. J. Rehr, Phys. Rev. B **69**, 125402 (2004); K. Hamalainen, S. Galambosi, J. A. Soininen, E. L. Shirley, J. P. Rueff, and A. Shukla, *ibid.* **65**, 155111 (2002); C. Sternemann, M. Volmer, J. A. Soininen, H. Nagasawa, M. Paulus, H. Enkisch, G. Schmidt, M. Tolan, and W. Schulke, *ibid.* **68**, 035111 (2003).
[22] J. A. Soininen, A. L. Ankudinov, and J. J. Rehr, Phys. Rev. B **72**, 045136 (2005).
[23] T. T. Fister, G. T. Seidler, C. Hamner, J. O. Cross, J. A. Soininen, and J. J. Rehr, Phys. Rev. B **74**, 214117 (2006).
[24] T. T. Fister, F. D. Vila, G. T. Seidler, L. Svec, J. C. Linehan, and J. O. Cross, J. Am. Chem. Soc. **130**, 925 (2008).
[25] S. Galambosi, M. Knaapila, J. A. Soininen, K. Nygard, S. Huotari, F. Galbrecht, U. Scherf, A. P. Monkman, and K. Hamalainen, Macromolecules **39**, 9261 (2006).
[26] R. A. Gordon, G. T. Seidler, T. T. Fister, M. W. Haverkort, G. A. Sawatzky, A. Tanaka, and T. K. Sham, Europhys. Lett. **81**, 26004 (2008).
[27] J. A. Soininen, A. Mattila, J. J. Rehr, S. Galambosi, and K. Hamalainen, J. Phys.: Condens. Matter **18**, 7327 (2006).
[28] C. Sternemann, J. A. Soininen, M. Volmer, A. Hohl, G. Vanko, S. Streit, and M. Tolan, J. Phys. Chem. Solids **66**, 2277 (2005).
[29] A. L. Ankudinov, B. Ravel, J. J. Rehr, and S. D. Conradson, Phys. Rev. B **58**, 7565 (1998).
[30] J. A. Soininen, K. Hamalainen, W. A. Caliebe, C. C. Kao, and E. L. Shirley, J. Phys.: Condens. Matter **13**, 8039 (2001).
[31] E. L. Shirley, J. A. Soininen, and J. J. Rehr (unpublished).
[32] E. L. Shirley, J. Electron Spectrosc. Relat. Phenom. **136**, 77 (2004); E. L. Shirley, Ultramicroscopy **106**, 986 (2006).
[33] E. L. Shirley, J. Electron Spectrosc. Relat. Phenom. **144–147**, 1187 (2005).
[34] E. L. Shirley, Phys. Rev. B **54**, 16464 (1996).
[35] D. R. Hamann, M. Schlüter, and C. Chiang, Phys. Rev. Lett. **43**, 1494 (1979).
[36] D. Vanderbilt, Phys. Rev. B **32**, 8412 (1985).
[37] E. L. Shirley, F. J. Himpsel, L. J. Terminello, and J. E. Klepeis, Phys. Rev. B **53**, 10296 (1996).
[38] G. Kresse and J. Furthmuller, Phys. Rev. B **54**, 11169 (1996).
[39] J. P. Perdew, K. Burke, and M. Ernzerhof, Phys. Rev. Lett. **77**, 3865 (1996).
[40] R. Bader, *Atoms in Molecules: A Quantum Theory* (Oxford University Press, New York, 1990).
[41] G. Henkelman, A. Arnaldsson, and H. Jonsson, Comput. Mater. Sci. **36**, 354 (2006).
[42] T. T. Fister, G. T. Seidler, L. Wharton, A. R. Battle, T. B. Ellis, J. O. Cross, A. T. Macrander, W. T. Elam, T. A. Tyson, and Q. Qian, Rev. Sci. Instrum. **77**, 063901 (2006).
[43] T. T. Fister, Ph.D. thesis, University of Washington, 2007.
[44] F. de Groot and A. Kotani, *Core Level Spectroscopy of Solids* (Taylor & Francis, London, 2008).
[45] P. A. Lee and J. B. Pendry, Phys. Rev. B **11**, 2795 (1975).
[46] J. J. Rehr and R. C. Albers, Rev. Mod. Phys. **72**, 621 (2000).